

# Probing the Epoch of Early Baryonic Infall Through 21cm Fluctuations

R. Barkana<sup>1</sup> and A. Loeb<sup>2</sup> \*

<sup>1</sup>*School of Physics and Astronomy, The Raymond and Beverly Sackler Faculty of Exact Sciences, Tel Aviv University, Tel Aviv 69978, ISRAEL*

<sup>2</sup>*Astronomy Department, Harvard University, 60 Garden Street, Cambridge, MA 02138, USA*

7 November 2018

## ABSTRACT

After cosmological recombination, the primordial hydrogen gas decoupled from the cosmic microwave background (CMB) and fell into the gravitational potential wells of the dark matter. The neutral hydrogen imprinted acoustic oscillations on the pattern of brightness fluctuations due to its redshifted 21cm absorption of the CMB. Unlike CMB temperature fluctuations which probe the power spectrum at cosmic recombination, we show that observations of the 21cm fluctuations at  $z \sim 20$ –200 can measure four separate fluctuation modes (with a fifth mode requiring very high precision), thus providing a unique probe of the geometry and composition of the universe.

**Key words:** galaxies:high-redshift – cosmology:theory – galaxies:formation

## 1 INTRODUCTION

Resonant absorption by neutral hydrogen at its spin-flip 21cm transition can be used to map its three-dimensional distribution at early cosmic times (Hogan & Rees 1979; Scott & Rees 1990; Madau et al. 1997). The primordial inhomogeneities in the cosmic gas induced variations in the optical depth for absorption of the cosmic microwave background (CMB) at the redshifted 21cm wavelength. Absorption occurs as long as the spin temperature of hydrogen,  $T_s$  (which characterizes the population ratio of the upper and lower states of the 21cm transition), is lower than the CMB temperature,  $T_\gamma$ . This condition is satisfied in the redshift interval  $20 \lesssim z \lesssim 200$  (Loeb & Zaldarriaga 2004), before the first galaxies formed in the universe (Barkana & Loeb 2001).

The formation of hydrogen through the recombination of protons and electrons at  $z \sim 10^3$  decoupled the cosmic gas from its mechanical drag on the CMB. Subsequently, the neutral gas was free to fall into the gravitational potential wells of the dark matter. The infalling gas retained some memory of the oscillations imprinted in the power spectrum of its density fluctuations on the scale traversed by sound waves in the photon-baryon fluid prior to decoupling. The signatures of these acoustic oscillations have been detected recently in the CMB anisotropies from  $z \sim 10^3$  (Spergel et al. 2003) and in the large-scale distribution of massive galaxies at  $z \sim 0.35$  (Eisenstein et al. 2005; Cole et al. 2005). Here we calculate their imprint on the

21cm brightness fluctuations at the intermediate range of  $20 \lesssim z \lesssim 200$  and propose it as a probe of the composition and geometry of the universe. Previous calculations of the fluctuations at these redshifts were inaccurate since they ignored fluctuations in the sound speed of the cosmic gas. Furthermore, we show that the 21cm power spectrum as a function of redshift can be decomposed into a combination of five fixed fluctuation modes, with coefficients that vary with redshift. We show that these modes and their coefficients can all be measured directly and then used to constrain cosmological parameters. Several groups are currently engaged in the construction of low-frequency radio experiments that will attempt to detect the diffuse 21cm radiation from  $z \gtrsim 6$  (<http://space.mit.edu/eor-workshop/>).

## 2 GROWTH OF DENSITY PERTURBATIONS

On large scales, the dark matter (dm) and the baryons (b) are affected only by their combined gravity. The evolution of sub-horizon linear perturbations is described by two coupled second-order differential equations (Peebles 1980):

$$\begin{aligned} \ddot{\delta}_{\text{dm}} + 2H\dot{\delta}_{\text{dm}} &= 4\pi G\bar{\rho}_m (f_b\delta_b + f_{\text{dm}}\delta_{\text{dm}}) , \\ \ddot{\delta}_b + 2H\dot{\delta}_b &= 4\pi G\bar{\rho}_m (f_b\delta_b + f_{\text{dm}}\delta_{\text{dm}}) , \end{aligned} \quad (1)$$

where  $\delta_{\text{dm}}(t)$  and  $\delta_b(t)$  are the perturbations in the dark matter and baryons, respectively, the derivatives are with respect to cosmic time  $t$ ,  $H(t) = \dot{a}/a$  is the Hubble constant with  $a = (1+z)^{-1}$ , and we assume that the mean mass density  $\bar{\rho}_m(t)$  is made up of respective mass fractions  $f_{\text{dm}}$  and  $f_b = 1 - f_{\text{dm}}$ . Since these linear equations contain no

\* E-mail: barkana@wise.tau.ac.il (RB); aloeb@cfa.harvard.edu (AL)

spatial gradients, they can be solved spatially for  $\delta_{\text{dm}}(\mathbf{x}, t)$  and  $\delta_{\text{b}}(\mathbf{x}, t)$  or in Fourier space for  $\tilde{\delta}_{\text{dm}}(\mathbf{k}, t)$  and  $\tilde{\delta}_{\text{b}}(\mathbf{k}, t)$ .

Defining  $\delta_{\text{tot}} \equiv f_{\text{b}}\delta_{\text{b}} + f_{\text{dm}}\delta_{\text{dm}}$  and  $\delta_{\text{b-}} \equiv \delta_{\text{b}} - \delta_{\text{tot}}$ , we find

$$\begin{aligned}\ddot{\delta}_{\text{tot}} + 2H\dot{\delta}_{\text{tot}} &= 4\pi G\bar{\rho}_m\delta_{\text{tot}}, \\ \ddot{\delta}_{\text{b-}} + 2H\dot{\delta}_{\text{b-}} &= 0.\end{aligned}\quad (2)$$

Each of these equations has two independent solutions. The equation for  $\delta_{\text{tot}}$  has the usual growing and decaying solutions, which we denote  $D_1(t)$  and  $D_4(t)$ , respectively, while the  $\delta_{\text{b-}}$  equation has solutions  $D_2(t)$  and  $D_3(t)$ ; we number the solutions in order of declining growth rate (or increasing decay rate). We assume an Einstein-de Sitter, matter-dominated universe in the redshift range  $z = 20$ – $150$ , since the radiation contributes less than a few percent at  $z < 150$ , while the cosmological constant and the curvature contribute to the energy density less than a few percent at  $z > 3$ . In this regime  $a \propto t^{2/3}$  and the solutions are  $D_1(t) = a/a_i$  and  $D_4(t) = (a/a_i)^{-3/2}$  for  $\delta_{\text{tot}}$ , and  $D_2(t) = 1$  and  $D_3(t) = (a/a_i)^{-1/2}$  for  $\delta_{\text{b-}}$ , where we have normalized each solution to unity at the starting scale factor  $a_i$ . Intuitively, since baryons and dark matter both feel the same gravity, the difference between them changes according to  $D_2$  and  $D_3$  which describe the evolution of perturbations in the absence of gravity. We set the initial redshift  $z_i = 150$ , when the photon density and temperature perturbations become negligible on sub-horizon scales and can be neglected (Naoz & Barkana 2005).

The observable baryon perturbation can then be written as

$$\tilde{\delta}_{\text{b}}(\mathbf{k}, t) = \tilde{\delta}_{\text{b-}} + \tilde{\delta}_{\text{tot}} = \sum_{m=1}^4 \tilde{\delta}_m(\mathbf{k}) D_m(t), \quad (3)$$

and similarly for the dark matter perturbation,

$$\tilde{\delta}_{\text{dm}} = \frac{1}{f_{\text{dm}}} (\tilde{\delta}_{\text{tot}} - f_{\text{b}}\tilde{\delta}_{\text{b}}) = \sum_{m=1}^4 \tilde{\delta}_m(\mathbf{k}) C_m(t), \quad (4)$$

where  $C_i = D_i$  for  $i = 1, 4$  and  $C_i = -(f_{\text{b}}/f_{\text{dm}})D_i$  for  $i = 2, 3$ . We establish the values of  $\tilde{\delta}_m(\mathbf{k})$  by inverting the  $4 \times 4$  matrix  $\mathbf{A}$  that relates the 4-vector  $(\tilde{\delta}_1, \tilde{\delta}_2, \tilde{\delta}_3, \tilde{\delta}_4)$  to the 4-vector that represents the initial conditions  $(\tilde{\delta}_{\text{b}}, \tilde{\delta}_{\text{dm}}, \dot{\tilde{\delta}}_{\text{b}}, \dot{\tilde{\delta}}_{\text{dm}})$  at the initial time.

### 3 GROWTH OF TEMPERATURE PERTURBATIONS

We include the (previously ignored) fluctuations in the sound speed of the cosmic gas caused by Compton heating of the gas, which is due to scattering of the residual electrons with the CMB photons. The evolution of the temperature  $T$  of a gas element of density  $\rho_b$  is given by the first law of thermodynamics:

$$dQ = \frac{3}{2}k_{\text{B}}dT - k_{\text{B}}T d \log \rho_b, \quad (5)$$

where  $dQ$  is the heating rate per particle. Before the first galaxies formed,

$$\frac{dQ}{dt} = 4 \frac{\sigma_{\text{T}} c}{m_e} k_{\text{B}}(T_{\gamma} - T)\rho_{\gamma}x_e(t), \quad (6)$$

where  $\sigma_{\text{T}}$  is the Thomson cross-section,  $x_e(t)$  is the electron fraction out of the total number density of gas particles, and  $\rho_{\gamma}$  is the CMB energy density at a temperature  $T_{\gamma}$ . In the redshift range of interest, we assume that the photon temperature ( $T_{\gamma} = T_{\gamma}^0/a$ ) is spatially uniform, since the high sound speed of the photons (i.e.,  $c/\sqrt{3}$ ) suppresses fluctuations on the sub-horizon scales that we consider, and the horizon-scale  $\sim 10^{-5}$  fluctuations imprinted at cosmic recombination are also negligible compared to the smaller-scale fluctuations in the gas density and temperature. Fluctuations in the residual electron fraction  $x_e(t)$  are even smaller. Thus,

$$\frac{dT}{dt} = \frac{2}{3}T \frac{d \log \rho_b}{dt} + \frac{x_e(t)}{t_{\gamma}} (T_{\gamma} - T) a^{-4}, \quad (7)$$

where  $t_{\gamma}^{-1} \equiv \bar{\rho}_{\gamma}^0(8\sigma_{\text{T}}c/3m_e) = 8.55 \times 10^{-13} \text{yr}^{-1}$ . After cosmic recombination,  $x_e(t)$  changes due to the slow recombination rate of the residual ions:

$$\frac{dx_e(t)}{dt} = -\alpha_{\text{B}}(T)x_e^2(t)\bar{n}_{\text{H}}(1+y), \quad (8)$$

where  $\alpha_{\text{B}}(T)$  is the case-B recombination coefficient of hydrogen,  $\bar{n}_{\text{H}}$  is the mean number density of hydrogen at time  $t$ , and  $y = 0.079$  is the helium to hydrogen number density ratio. This yields the evolution of the mean temperature,  $d\bar{T}/dt = -2H\bar{T} + x_e(t)t_{\gamma}^{-1}(T_{\gamma} - \bar{T})a^{-4}$ . In prior analyses (e.g., Peebles 1980; Ma & Bertschinger 1995) a spatially uniform speed of sound was assumed for the gas at each redshift. Note that we refer to  $\delta p/\delta \rho$  as the square of the sound speed of the fluid, where  $\delta p$  is the pressure perturbation, although we are analyzing perturbations driven by gravity rather than sound waves driven by pressure gradients.

Instead of assuming a uniform sound speed, we find the first-order perturbation equation,

$$\frac{d\delta_T}{dt} = \frac{2}{3} \frac{d\delta_{\text{b}}}{dt} - \frac{x_e(t)}{t_{\gamma}} \frac{T_{\gamma}}{T} a^{-4} \delta_T, \quad (9)$$

where we defined the fractional temperature perturbation  $\delta_T$ . Like the density perturbation equations, this equation can be solved separately at each  $\mathbf{x}$  or at each  $\mathbf{k}$ . Furthermore, the solution  $\delta_T(t)$  is a linear functional of  $\delta_{\text{b}}(t)$  [for a fixed function  $x_e(t)$ ]. Thus, if we choose an initial time  $t_i$  then using Eq. (3) we can write the solution in Fourier space as

$$\tilde{\delta}_T(\mathbf{k}, t) = \sum_{m=1}^4 \tilde{\delta}_m(\mathbf{k}) D_m^T(t) + \tilde{\delta}_T(\mathbf{k}, t_i) D_0^T(t), \quad (10)$$

where  $D_m^T(t)$  is the solution of Eq. (9) with  $\delta_T = 0$  at  $t_i$  and with the perturbation mode  $D_m(t)$  substituted for  $\delta_{\text{b}}(t)$ , while  $D_0^T(t)$  is the solution with no perturbation  $\delta_{\text{b}}(t)$  and with  $\delta_T = 1$  at  $t_i$ . By modifying the CMBFAST code (Seljak & Zaldarriaga 1996), we numerically solve Eq. (9) along with the density perturbation equations for each  $\mathbf{k}$  down to  $z_i = 150$ , and then match the solution to the form of Eq. (10). We note that Bharadwaj & Ali (2004a) derived a similar equation to Eq. (9) but solved it only for a density perturbation that follows the growing mode  $D_1(t)$ , neglecting the other density modes and the initial temperature perturbation.

Figure 1 shows the time evolution of the various independent modes that make up the perturbations of density and temperature, starting at the time  $t_i$  corresponding to  $z_i = 150$ .  $D_2^T(t)$  is identically zero since  $D_2(t) = 1$

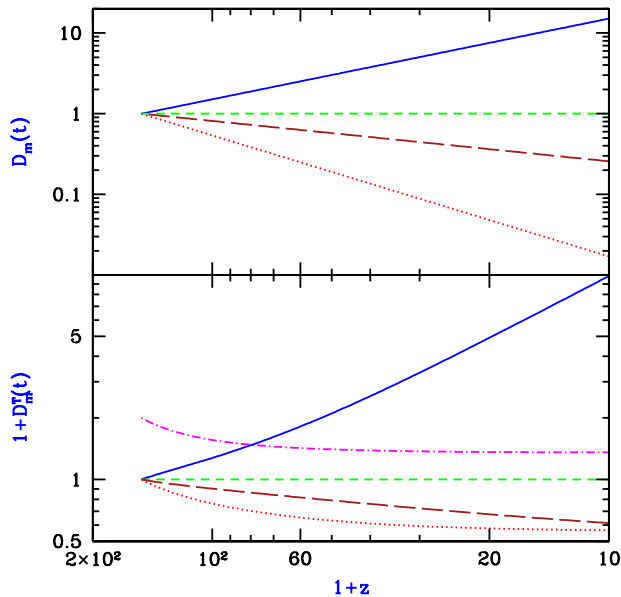


**Figure 1.** Redshift evolution of the amplitudes of the independent modes of the density perturbations (upper panel) and the temperature perturbations (lower panel), starting at redshift 150. We show  $m = 1$  (solid curves),  $m = 2$  (short-dashed curves),  $m = 3$  (long-dashed curves),  $m = 4$  (dotted curves), and  $m = 0$  (dot-dashed curve). Note that the lower panel shows one plus the mode amplitude.

is constant, while  $D_3^T(t)$  and  $D_4^T(t)$  are negative. Figure 2 shows the amplitudes of the various components of the initial perturbations. We consider comoving wavevectors  $k$  in the range  $0.01 - 40 \text{ Mpc}^{-1}$ , where the lower limit is set by considering sub-horizon scales at  $z = 150$  for which photon perturbations are negligible compared to  $\delta_{\text{dm}}$  and  $\delta_{\text{b}}$ , and the upper limit is set by requiring baryonic pressure to be negligible compared to gravity.  $\delta_2$  and  $\delta_3$  clearly show a strong signature of the large-scale baryonic oscillations, left over from the era of the photon-baryon fluid before recombination, while  $\delta_1$ ,  $\delta_4$ , and  $\tilde{\delta}_T$  carry only a weak sign of the oscillations. For each quantity, the plot shows  $[k^3 P(k)/(2\pi^2)]^{1/2}$ , where  $P(k)$  is the corresponding power spectrum of fluctuations.

$\tilde{\delta}_4$  is already a very small correction at  $z = 150$  and declines quickly at lower redshift, but the other three modes all contribute significantly to  $\tilde{\delta}_{\text{b}}$ , and the  $\tilde{\delta}_T(t_i)$  term remains significant in  $\tilde{\delta}_T(t)$  even at  $z \lesssim 100$ . Note that at  $z = 150$  the temperature perturbation  $\tilde{\delta}_T$  has a different shape with respect to  $k$  than the baryon perturbation  $\tilde{\delta}_{\text{b}}$ , showing that their ratio cannot be described by a scale-independent speed of sound.

The power spectra of the various perturbation modes and of  $\tilde{\delta}_T(t_i)$  depend on the initial power spectrum of density fluctuations from inflation and on the values of the fundamental cosmological parameters ( $\Omega_{\text{dm}}$ ,  $\Omega_{\text{b}}$ ,  $\Omega_{\Lambda}$ , and  $h$ ). If these independent power spectra can be measured through 21cm fluctuations, this will probe the basic cosmological parameters through multiple combinations, allowing consistency checks that can be used to verify the adiabatic nature and the expected history of the perturbations. Figure 3 il-

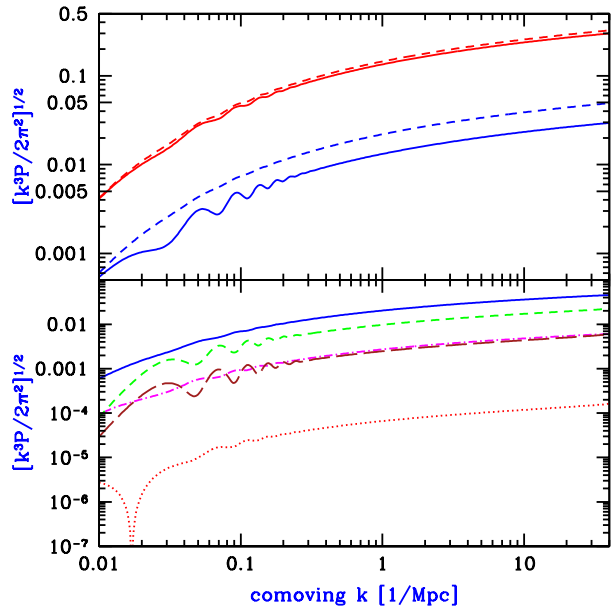


**Figure 2.** Power spectra and initial perturbation amplitudes versus wavenumber. The upper panel shows  $\tilde{\delta}_{\text{b}}$  (solid curves) and  $\tilde{\delta}_{\text{dm}}$  (dashed curves) at  $z = 150$  and  $20$  (from bottom to top). The lower panel shows the initial ( $z = 150$ ) amplitudes of  $\tilde{\delta}_1$  (solid curve),  $\tilde{\delta}_2$  (short-dashed curve),  $\tilde{\delta}_3$  (long-dashed curve),  $\tilde{\delta}_4$  (dotted curve), and  $\tilde{\delta}_T(t_i)$  (dot-dashed curve). Note that if  $\tilde{\delta}_1$  is positive then so are  $\tilde{\delta}_3$  and  $\tilde{\delta}_T(t_i)$ , while  $\tilde{\delta}_2$  is negative at all  $k$ , and  $\tilde{\delta}_4$  is negative at the lowest  $k$  but is positive at  $k > 0.017 \text{ Mpc}^{-1}$ .

lustrates the relative sensitivity of  $\sqrt{P(k)}$  to variations in  $\Omega_{\text{dm}} h^2$ ,  $\Omega_{\text{b}} h^2$ , and  $h$ , for the quantities  $\tilde{\delta}_1$ ,  $\tilde{\delta}_2$ ,  $\tilde{\delta}_3$ , and  $\tilde{\delta}_T(t_i)$ . Not shown is  $\tilde{\delta}_4$ , which although it is more sensitive (changing by order unity due to 10% variations in the parameters), its magnitude always remains much smaller than the other modes, making it much harder to detect. Note that although the angular scale of the baryon oscillations constrains also the history of dark energy through the angular diameter distance, we have focused here on other cosmological parameters, since the contribution of dark energy relative to matter becomes negligible at high redshift.

## 4 21CM FLUCTUATIONS

The spin temperature  $T_s$  is defined through the ratio between the number densities of hydrogen atoms,  $n_1/n_0 = (g_1/g_0) \exp\{-T_*/T_s\}$ , where subscripts 1 and 0 correspond to the excited and ground state levels of the 21cm transition,  $(g_1/g_0) = 3$  is the ratio of the spin degeneracy factors of the levels, and  $T_* = 0.0682\text{K}$  corresponds to the energy difference between the levels. The 21cm spin temperature is on the one hand radiatively coupled to the CMB temperature, and on the other hand coupled to the kinetic gas temperature  $T$  through collisions (Allison & Dalgarno 1969) or the absorption of Ly $\alpha$  photons (Wouthuysen 1952; Field 1958). For the concordance set of cosmological parameters (Spergel et al. 2003), the mean brightness temperature on the sky at redshift  $z$  (relative to the CMB itself) is (Madau et al. 1997)

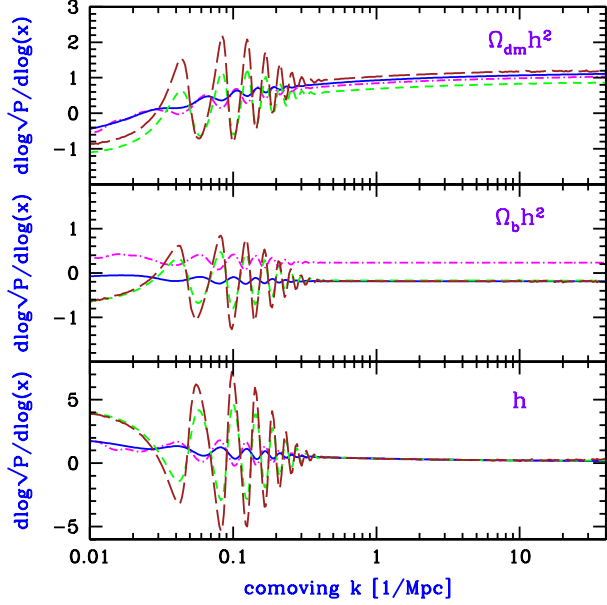


**Figure 3.** Relative sensitivity of perturbation amplitudes at  $z = 150$  to cosmological parameters. For variations in a parameter  $x$ , we show  $d \log \sqrt{P(k)}/d \log(x)$ . We consider variations in  $\Omega_{\text{dm}} h^2$  (upper panel), in  $\Omega_b h^2$  (middle panel), and in the Hubble constant  $h$  (lower panel). When we vary each parameter we fix the other two, and the variations are all carried out in a flat  $\Omega_{\text{total}} = 1$  universe. We show the sensitivity of  $\tilde{\delta}_1$  (solid curves),  $\tilde{\delta}_2$  (short-dashed curves),  $\tilde{\delta}_3$  (long-dashed curves), and  $\tilde{\delta}_T(t_i)$  (dot-dashed curves).

$T_b = 28 \text{ mK} [(1+z)/10]^{1/2} [(T_s - T_\gamma)/T_s] \bar{x}_{\text{HI}}$ , where  $\bar{x}_{\text{HI}}$  is the mean neutral fraction of hydrogen.

In general, fluctuations in  $T_b$  can be sourced by fluctuations in gas density, temperature, neutral fraction, radial velocity gradient, and Ly $\alpha$  flux from galaxies. The velocity gradient term (Sobolev 1960) is in Fourier space (Kaiser 1987; Bharadwaj & Ali 2004a,b)  $\tilde{\delta}_{d_r v_r} = -\mu^2 \tilde{\delta}/H$ , where  $\mu = \cos \theta_k$  in terms of the angle  $\theta_k$  of  $\mathbf{k}$  with respect to the line of sight. We can therefore write the fluctuation as (Barkana & Loeb 2005)

$$\tilde{\delta}_{T_b}(\mathbf{k}, t) = \mu^2 \tilde{\delta}(\mathbf{k}) H^{-1} + \beta \tilde{\delta}(\mathbf{k}) + \beta_T \tilde{\delta}_T(\mathbf{k}) + \tilde{\delta}_{\text{rad}}(\mathbf{k}), \quad (11)$$

where we have defined time-dependent coefficients  $\beta$  and  $\beta_T$  (combining the relevant explicit terms from Eq. 2 of Barkana & Loeb (2005)), and have also combined the terms that depend on the radiation fields of Ly $\alpha$  photons and ionizing photons into  $\tilde{\delta}_{\text{rad}}$ . Before the first galaxies formed,  $\bar{x}_{\text{HI}} = 1$  and  $\tilde{\delta}_{\text{rad}} = 0$ . Thus,

$$\tilde{\delta}_{T_b}(\mathbf{k}, t) = \sum_{m=1}^4 \tilde{\delta}_m(\mathbf{k}) [\mu^2 H^{-1}(t) \dot{D}_m(t) + \beta D_m(t) + \beta_T D_m^T(t)] + \beta_T \tilde{\delta}_T(\mathbf{k}, t_i) D_0^T(t). \quad (12)$$

The power spectrum  $P_{T_b}$  is defined by

$$\langle \tilde{\delta}_{T_b}(\mathbf{k}_1, t) \tilde{\delta}_{T_b}^*(\mathbf{k}_2, t) \rangle = (2\pi)^3 \delta^D(\mathbf{k}_1 + \mathbf{k}_2) P_{T_b}(\mathbf{k}_1, t). \quad (13)$$

At  $z = 150$ , the overall contributions of the  $\tilde{\delta}_1$ ,  $\tilde{\delta}_2$ ,  $\tilde{\delta}_3$ , and  $\tilde{\delta}_T(t_i)$  terms to  $P_{T_b}$  are comparable, while the  $\tilde{\delta}_4$  term (which corresponds to the usual decaying mode) represents only a

1% correction to the 21cm power spectrum. The contributions of the different terms to  $\tilde{\delta}_{T_b}$  then scale with redshift roughly like the corresponding density modes  $D_m(t)$ , with the  $\tilde{\delta}_T(t_i)$  term varying roughly as  $\propto 1/a$ , so that the usual growing mode  $\tilde{\delta}_1$  dominates at low redshift.

Noting that observations of the 21cm power spectrum can be analyzed as a function of  $k$  and  $\mu$ , we write the power spectrum as a polynomial in  $\mu$  (Barkana & Loeb 2005),

$$P_{T_b}(\mathbf{k}) = \mu^4 P_{\mu^4}(k) + \mu^2 P_{\mu^2}(k) + P_{\mu^0}(k), \quad (14)$$

and obtain the three separate power spectra of 21cm fluctuations. Figure 4 shows their values at various redshifts. The fluctuations rise with time until  $z \sim 50$  due to the growth of fluctuations and then decline at lower redshift due to the reduced collisional coupling of the 21cm spin temperature to the gas temperature (Loeb & Zaldarriaga 2004). The five power spectra shown in the lower panel of Fig. 2 along with the coefficients of the five modes in Eq. (12) can all be determined directly from observations. Suppose, e.g., that we measure the three observable power spectra at  $N$   $k$ -values at  $M$  different redshifts, for a total of  $3NM$  data points. As we have shown, these data points can be modeled in terms of the amplitudes of five separate fluctuation modes at the same  $N$   $k$ -values, along with two coefficients per redshift for each fluctuation mode [corresponding to the contributions to the  $\mu^2$  term and to the  $\mu$ -independent term in Eq. (12)]. The total of  $5N + 10M$  parameters can then be determined as long as the number of data points is larger than this total. Thus,  $M = 4$  redshifts suffice as long as  $N \geq 5$ , while  $M = 2$  suffices for any  $N \geq 20$ . Measurements at additional redshifts will allow a more accurate reconstruction along with multiple consistency checks. Note that Figure 1 shows that separating out the different modes at  $z \sim 20$  requires an order of magnitude higher measurement precision than at  $z \sim 100$ .

Detection of these fluctuations with future experiments (Zaldarriaga et al. 2004; Morales & Hewitt 2004; Morales 2005) would set new constraints on the evolution of the universe through a regime of cosmic time that has never been probed before. Unlike existing cosmological probes, the three-dimensional nature of 21cm fluctuations makes possible measurements at a wide range of redshifts and scales. CMB temperature fluctuations (Spergel et al. 2003) probe the power spectrum only at cosmic recombination, and only on scales  $k \leq 0.2 \text{ Mpc}^{-1}$  which are not damped by photon diffusion. Galaxy redshift surveys (Tegmark et al. 2004; Cole et al. 2005) probe the density power spectrum only at low redshifts where the fastest-growing mode  $D_1(t)$  is already strongly dominant, and the signature of the baryonic oscillations is weak. Furthermore, even on large scales ( $k < 0.1 \text{ Mpc}^{-1}$ ) the biased distribution of galaxies may be affected by complex astrophysical feedback processes such as cosmic reionization (Barkana & Loeb 2004).

Indeed, CMB fluctuations and galaxy surveys cannot individually constrain multiple-parameter cosmological models due to degeneracies, and must be combined in order to achieve significant constraints (Tegmark et al. 2004). In contrast, 21cm fluctuations provide a signal at a sufficiently early epoch when the baryons have not yet caught up with the dark matter, and four separate fluctuation modes are detectable (with a fifth mode requiring higher precision). Since each mode depends differently on the cosmological param-

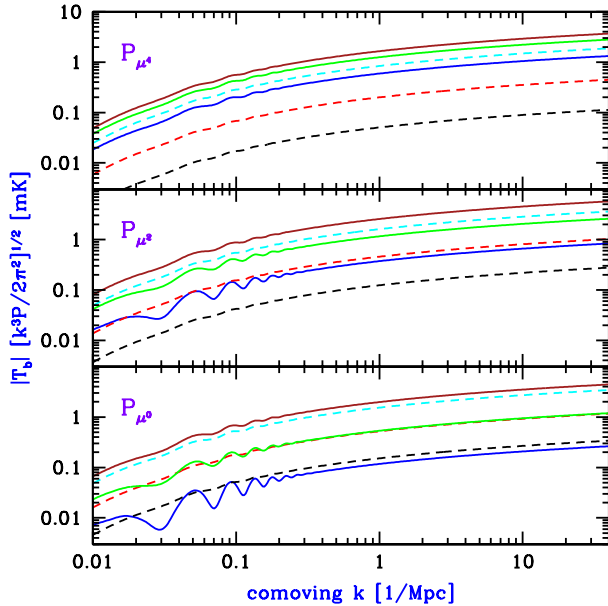


**Figure 4.** Power spectra of 21cm brightness fluctuations versus wavenumber. We show the three power spectra that are separately observable,  $P_{\mu^4}$  (upper panel),  $P_{\mu^2}$  (middle panel), and  $P_{\mu^0}$  (lower panel). In each case we show redshifts 150, 100, 50 (solid curves, from bottom to top), 35, 25, and 20 (dashed curves, from top to bottom).

eters (see Fig. 3), such measurements would provide great discriminatory power in determining the cosmological parameters and in testing for any deviations from the standard  $\Lambda$ CDM paradigm. This cosmological information is in principle available from measurements in any redshift range, but the amplitudes of some of the modes decline at low redshift and they become more challenging to measure (see Fig. 1). While we have focused on deriving constraints from the power spectra, we note that the coefficients in Eq. (12) depend on known cosmological and atomic physics, so that measuring them from the 21cm data will help to further constrain the fundamental cosmological parameters.

## ACKNOWLEDGMENTS

This work was supported in part by NSF grants AST-0204514, AST-0071019 and NASA grant NAG 5-13292. R.B. acknowledges the support of Israel Science Foundation grant 28/02/01.

## REFERENCES

- Allison, A. C., & Dalgarno, A. 1969, *ApJ*, 158, 423  
 Barkana, R., & Loeb, A. 2001, *Phys. Rep.*, 349, 125  
 ———. 2004, *ApJ*, 609, 474  
 ———. 2005, *ApJ*, submitted [astro-ph/0409572]  
 Bharadwaj, S., & Ali, S. S. 2004a, *MNRAS*, 352, 142  
 Bharadwaj, S., & Ali, S. S. 2004b, *MNRAS*, 356, 1519  
 Cole, S., et al. 2005, *MNRAS*, submitted [astro-ph/0501174]

- Eisenstein, D., et al. 2005, *ApJ*, submitted [astro-ph/0501171]  
 Field, G. B. 1958, *Proc. IRE*, 46, 240  
 Hogan, C. J., & Rees, M. J. 1979, *MNRAS*, 188, 791  
 Kaiser, N. 1987, *MNRAS*, 227, 1  
 Loeb, A., & Zaldarriaga, M. 2004, *Phys. Rev. Lett.*, 92, 211301  
 Ma, C. & Bertschinger, E. 1995, *ApJ*, 455, 7  
 Madau, P., Meiksin, A., & Rees, M. J. 1997, *ApJ*, 475, 429  
 Morales, M. F. 2005, *ApJ*, 619, 678  
 Morales, M. F., & Hewitt, J. 2004, *ApJ*, 615, 7  
 Naoz, S., & Barkana, R. 2005, *MNRAS*, submitted [astro-ph/0503196]  
 Peebles, P. J. E. 1980, *The large-scale structure of the universe*, Princeton U. Press: Princeton  
 Scott, D. & Rees, M. J. 1990, *MNRAS*, 247, 510  
 U., Seljak, & M., Zaldarriaga 1996, *ApJ*, 469, 437; see <http://www.cmbfast.org>  
 Sobolev, V. V. 1960, *Moving Envelopes of Stars*, Cambridge: Harvard University Press  
 Spergel, D. N., et al. 2003, *ApJS*, 148, 175  
 Tegmark, M., et al. 2004, *ApJ*, 606, 702  
 Tegmark, M., et al. 2004, *PRD*, 69, 103501  
 Wouthuysen, S. A., 1952, *AJ*, 57, 31  
 Zaldarriaga, M., Furlanetto, S. R., & Hernquist, L. 2004, *ApJ*, 608, 622

This paper has been typeset from a  $\text{\TeX}/\text{\LaTeX}$  file prepared by the author.